

Scintillation detectors of Alborz-I experiment

Y. Pezeshkian^{a,b}, M. Bahmanabadi^{a,b,*}, M. Abbasian Motlagh^b, M. Rezaie^b

^a*Department of Physics, Sharif University of Technology, P.O.Box 11155-9161, Tehran, Iran*

^b*Alborz Observatory, Sharif University of Technology, P.O.Box 11155-9161, Tehran, Iran*

Abstract

A new air shower experiment of the Alborz Observatory, Alborz-I, located at the Sharif University of Technology, Iran, will be constructed in near future. An area of about $30 \times 40 \text{ m}^2$ will be covered by 20 plastic scintillation detectors (each with an area of $50 \times 50 \text{ cm}^2$). A series of experiments have been performed to optimize the height of light enclosures of the detectors for this array and the results have been compared to an extended code simulation of these detectors. Operational parameters of the detector obtained by this code are cross checked by Geant4 simulation. There is a good agreement between extended-code and Geant4 simulations. We also present further discussions on the detector characteristics, which can be applicable for all scintillation detectors with a similar configuration.

Keywords: Cosmic rays, Scintillation detectors, Ground based arrays

PACS: 95.55.Vj, 95.85.Ry, 95.75.-z, 29.40.Mc

1. Introduction

Nowadays scintillators are among important detectors used in many cosmic ray and high energy physics experiments. For instance, they are a major part of detectors in balloon experiments for the detection of cosmic rays; such as TIGER, CREAM and TRACER [1]. Liquid scintillators are used in several neutrino experiments, such as Borexino and KamLAND and in the next generation neutrino experiment LENA [2].

Scintillators at ground based arrays are used in different configurations. Liquid scintillators with pyramidal light enclosure and PhotoMultiplier Tube (PMT) at the vertex are used in KASCADE array [3]. In many experiments the plastic scintillators are connected to PMTs with optical fibers as light guide and wavelength shifter (WLS), e.g., Telescope array [4], KASCADE-Grande [5], and LHAASO [6]. Detectors in experiments of Tibet [7] and GRAPES3 [8]

*Corresponding author

Email address: bahmanabadi@sharif.edu (M. Bahmanabadi)

enclose plastic scintillators in pyramidal light enclosures. Both of these experiments also have scintillation detectors with optical fibers[7, 18]. Time resolution of scintillators with light enclosure is better than scintillators with WLS fiber readouts, since WLS has a large contribution in time resolution due to the decay time of WLS. On the other hand, scintillators with WLS provide more uniformity compared to light enclosures. Choosing detectors' configuration depends on the requirements of the experiment and the budget restrictions.

The Alborz air shower observatory at the Sharif University of Technology ($35^{\circ}43'N$, $51^{\circ}20'E$, 1200 m a.s.l, 890 g cm^{-2}) will have 30 installed detectors (20 scintillators and 10 Cherenkov detectors). The project is planned to be accomplished in 2 stages. At first stage (Alborz-I), the scintillation detectors with the area of $50 \times 50\text{ cm}^2$ will be placed on the rooftop of the highest building of the university campus. Detectors will be arranged in a square lattice with a side of $\sim 7\text{ m}$ (Fig.1(a)). Required electronics have already been prepared and primary tests will be accomplished in future. The aim of Alborz-I is to study extensive air showers (EAS) with energies around the knee region of the cosmic rays spectrum. Later, by adding more detectors, energy regions above the knee will be investigated. Primary studies, like detailed simulation of array configuration and distance between detectors, are under investigation. Cherenkov detectors will be added at second stage. Dimensions and some properties of Cherenkov detectors are optimized and the results were published in [9]. Detailed studies of scintillation detectors and related optimizations are subject of this paper.

In the former arrays of the Alborz observatory [10, 11, 12], the size of the scintillators was $100 \times 100\text{ cm}^2$ and the performance of these scintillators had studied in [13]. In order to improve the accuracy of the array in determining directions of cosmic rays, the size of detectors is reduced to $50 \times 50\text{ cm}^2$. By resizing the scintillators, light enclosure heights should also be optimized to obtain suitable signals. Beside height optimization of the light enclosures, we will also present the further results on the performance of these detectors including time response, uniformity, and effect of walls of the light enclosure.

In order to find the best height for the light enclosures, three different light enclosures are built and compared by experiment. Experimental set-up and procedure is explained and corresponding results are discussed in section 2. Section 3 with three subsections is dedicated to explain an extended-code simulation of Alborz-I scintillators. We describe details of the algorithm at the first subsection. In the second subsection, we present the simulation results including time spectrum of photons reaching PMT, the effect of light enclosure walls on the total number of captured photons, and other parameters of the detectors. At the third subsection, in order to cross check our extended code simulation, we compare time spectrum of photons reaching PMT obtained by Extended-code with a Geant4 simulation. we conclude that they have similar results for the same initial conditions. Some further discussions about time resolution of detectors are also presented in this subsection.

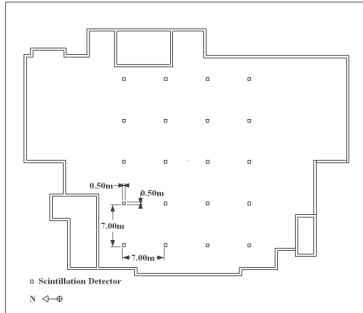
2. Experimental setup and Results

The detectors of the Alborz I observatory are plane plastic scintillators (NE102A) which are enclosed in a pyramidal light enclosure with a 5 cm photomultiplier tube (PMT, 9813B) at the vertex of the light enclosure (Fig. 1(b)). In order to optimize the height of the light enclosure, two parameters are important: total efficiency of the detector, and its uniformity. Uniformity requirement can be satisfied when the detection parameters (i.e., total number of events in the cells and their time resolutions) encounter little variation from center to the edge of the detector.

If the height of the enclosure is small, the PMT is very close to the center of the scintillator (and consequently far from the corners), therefore it is not possible to have an acceptable uniformity. By increasing the height of the light enclosure, uniformity of the detector from center (cell 1 in Fig. 1(c)) to corner (cell 6 in Fig. 1(c)) improves, but count rate of particles (i.e., the efficiency) decreases. To determine the optimum height, three light enclosures with heights of 10 cm, 20 cm, and 30 cm were made and a series of experiments for each of them were carried out.

The bottom surface of the scintillator is divided into 25 cells, each of them with the area $10 \times 10 \text{ cm}^2$, as shown in Fig. 1. Due to symmetry, it suffices to choose only six cells (cells 1-6 in Fig. 1(c)), and sweep them by a smaller scintillator ($10 \times 10 \times 0.5 \text{ cm}^3$) and accumulate the coincidence of the events for each cell and the small scintillator. In all experiments, the time lag between signals of these two scintillators is measured. Fig. 1(d) displays the scheme of the electronics in more detail, including fast discriminator (Disc., N413A), Time-to-Amplitude Converter (TAC, ORTEC566), and Analogue-to-Digital converter (ADC, KIAN AFROUZ). Output of this circuit is the time lag of the passage of a cosmic ray through both detectors. Overall run time of the experiment for 3 heights and 6 cells was $3 \times 6 \times 22 \text{ h}$. Temperature fluctuation was negligible during one month of the experiment, therefore, the effect of temperature and pressure fluctuations on the cosmic ray flux is not considered.

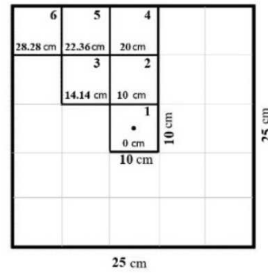
A sample of the time lag distribution of particles passing through two detectors is shown in Fig. 2. In this spectrum, each count is a start-stop event recorded by the Time-to-Amplitude Converter (TAC), which was set at a full scale of 200 ns, and corresponds to the passage of a cosmic ray through both scintillators in our experimental setup. The main differences in the spectra are the number of total counts under the peak, and the width of the peak. In computing the total counts under the peak for each spectrum, very low background counts (obtained from channels far from the peaks) have been subtracted. The width of each peak shows the time resolution. In extensive air shower experiments, which employ the large area scintillators and the light enclosures viewed by a single PMT, the uncertainty in transit time measurement produces an error in determining the arrival direction of the total shower. This transit time error component is in addition to the uncertainty in the transit position in the large area scintillator. The width of each peak is interpreted as an inherent timing error due to the light enclosures and the electronic devices. The Full



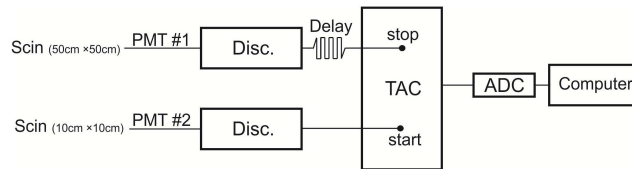
(a)



(b)



(c)



(d)

Figure 1: (a) A schematic view of Alborz-I array, (b) A sample of the Alborz-I scintillation detectors, (c) 6 swept cells of scintillator surface; the number in each cell is distance from the center of the detector, and (d) electronic circuit for data Read out.

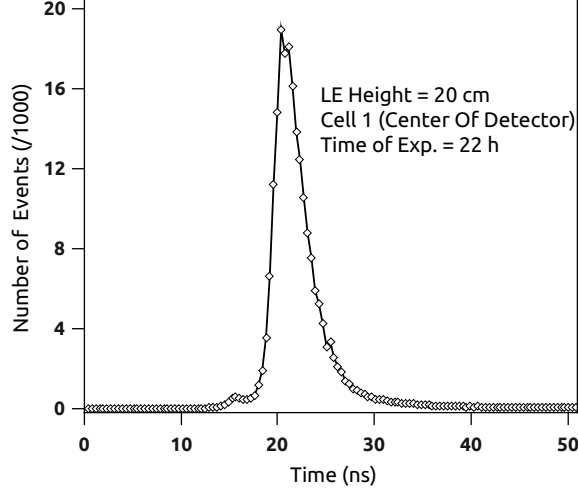


Figure 2: A sample of time lag distributions.

Width Half Maximum (FWHM) of each time lag distribution can be obtained by fitting a Gaussian function to it (Fig. 2). The uniformity of each detector can be evaluated by comparing the FWHM (Γ) and the efficiency (ε) values of its different cells.

Fig. 3 shows the total counts in each cell for heights of 10 cm, 20 cm, and 30 cm light enclosure. This figure shows a considerable non-uniformity in total counts in different cells.

In Fig. 4, we show the Γ value of each cell as a function of the cell distance from the PMT, for three heights. Equations of the fitted lines are also shown in the figure and the slope of each line is available in table 1. The statistical errors are not visible in Fig. 4, since they are smaller than the data points, but the deviations of the points from the lines are arisen due to asymmetry of the pyramidal light enclosure as a systematic error. In the case of 10 cm light enclosure, slope of the line is 0.11 ns/cm, which means that the FWHM of the time lag distributions increases significantly from the center to the corner of the detector (about 2.26 ns).

Mean value of FWHM for each height of the light enclosure can be calculated using the following equation:

$$\bar{\Gamma} = \frac{1}{\sum_{j=1}^6 m_j N_i} \sum_{j=1}^6 m_i N_i \Gamma_i; \quad (1)$$

where the summation is over the 6 swept cells (Fig. 1(c)), N_i is the total number of events in the cell i (Fig. 3) and m_i shows number of cells similar to the cell i on the total surface of the scintillator (that is $m_1 = 1$, $m_5 = 8$, and $m_i = 4$ for

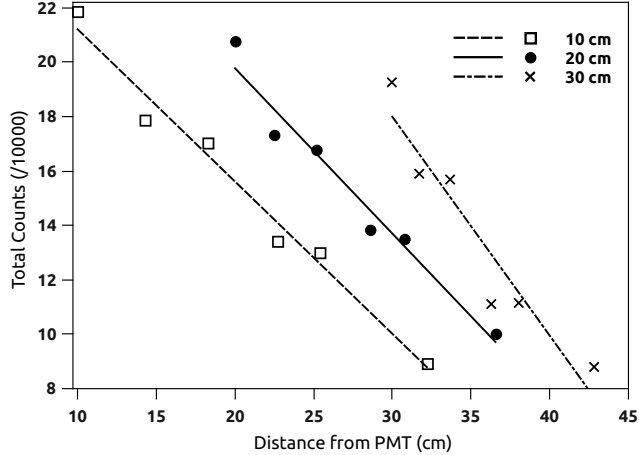


Figure 3: Total counts in each cell as a function of distance between corresponding cell and PMT for 3 light enclosures.

the rest of the cells). It is clear that the lower value of $\bar{\Gamma}$ indicates better time response of the detector. Therefore, the 20 cm light enclosure with FWHM of 4.35 ns has the best time resolution (Table 1).

In addition to these two parameters ($\bar{\Gamma}$ and the slope of Γ), the total number of events (i.e $\sum m_i N_i$), is another criterion for comparing the different light enclosures. Since the rate of cosmic rays is constant, one expects the number of particles crossing surfaces with equal areas ($10 \times 10 \text{ cm}^2$) at equal times (22 hours) to be the same. We assume the number of particles passing through each cell (N_T) is the same for all cells, namely, the flux of particles does not change during one month. The efficiency of the cell i is defined as $\varepsilon_i = N_i/N_T$, where N_i is the number of recorded particles in the cell i . The mean efficiency of the detector could be obtained as a function of the efficiency of cell in which it is maximum (in our case the cell 1 of the 10 cm light enclosure):

$$\bar{\varepsilon} = \frac{1}{\sum_{i=1}^6 m_i} \sum_{i=1}^6 \frac{m_i N_i}{N_{1,10}} \varepsilon_0 \times 100; \quad (2)$$

where $N_{1,10}$ and $\varepsilon_0 = \frac{N_{1,10}}{N_T}$ are number of events and efficiency of the cell 1 with the 10 cm light enclosure, respectively.

Results of the experiment (Table 1) show that the 20 cm light enclosure has a better efficiency and its mean value of FWHM ($\bar{\Gamma}$) is smaller compared to the 10 cm and 30 cm light enclosures. If the uniformity is the main concern, the 30 cm light enclosure should be chosen, however, because of its lower efficiency and higher $\bar{\Gamma}$, this light enclosure is not suitable. Therefore a 20 cm height is selected for the light enclosure of the detector.

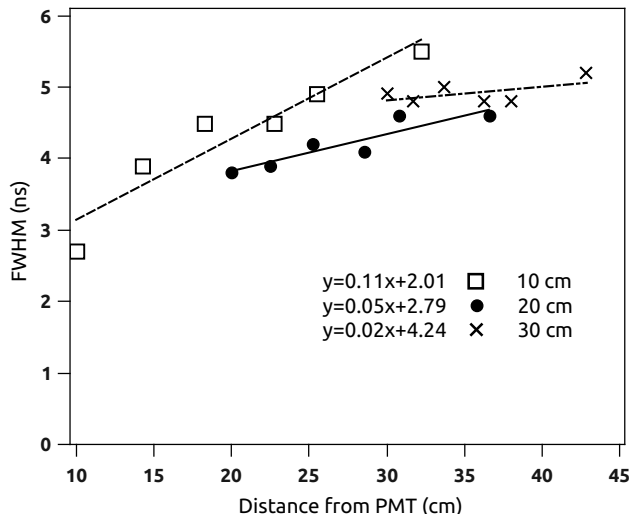


Figure 4: FWHM of each cell as a function of distance between corresponding cell and PMT for 3 light enclosures. Since the error bars are smaller than the data points, they are omitted.

Height(cm)	$\bar{\varepsilon}$ (%)	$\bar{\Gamma}$ (ns)	slope of Γ (ns cm^{-1})
10	$(64.9 \pm 1.6) \varepsilon_0$	4.73 ± 0.09	0.11
20	$(66.0 \pm 1.6) \varepsilon_0$	4.35 ± 0.08	0.05
30	$(57.5 \pm 1.4) \varepsilon_0$	5.01 ± 0.11	0.02

Table 1: $\bar{\varepsilon}$, $\bar{\Gamma}$ (ns) and Slope of Γ (ns cm^{-1}) for various heights of the light enclosures.

3. Simulation

3.1. Algorithm

A simulation of what happens in the detectors enables us to understand the detection process in more detail. When a charged particle passes through the detector, it loses some or all of its kinetic energy in the scintillator. Small fraction of the lost energy will be converted into fluorescent light and the remainder will be dissipated nonradiatively, primarily in the form of lattice vibrations and heat [14]. The number of scintillation photons can be calculated by using the light yield of the scintillator (available in the literature). In the simulation we use the properties of the scintillators of our experiment i.e., NE102A.

For the energy loss of a charged particle, dE/dx , in the scintillator, we use the value 2 MeV cm^{-1} , which is consistent with $\rho^{-1} dE/dx = 2 \text{ MeV}/(\text{gcm}^{-2})$ [15], and the density of NE102A, $\rho = 1.032 \text{ g cm}^{-3}$ [16].

Since light yield of NE102A is $10,000 \text{ photons MeV}^{-1}$ [14], about 20,000 photons will be emitted through each cm of the scintillator. A scintillator does

not emit all photons simultaneously, hence the profile of the light pulse of the scintillator should be considered. The distribution function of the emission time of photons is given by:

$$I = I_0(e^{-t/\tau_1} - e^{-t/\tau_2}); \quad (3)$$

where τ_1 and τ_2 are equal to 2.4 ns and 0.6 ns, respectively [14].

For each photon, the emission time can be assigned by using Monte Carlo method. In order to reduce run time of the program, emission time of photons is calculated only for photons reaching PMT, after finishing other steps of the simulation.

Each emitted photon chooses a stochastic direction and passes inside the detector. It is annihilated by two ways: (1) absorption by the inner surfaces of the light enclosure or its bottom surface (i.e., the surface directly beneath the large area scintillator), and (2) attenuation inside the plastic scintillator. The inner surface of the light enclosure is diffuse white, and its bottom surface is made of aluminium foil. By Diffuse Reflectance Spectroscopy (DRS) test, their absorption coefficients are about 0.2 and 0.1, respectively. A signal can be produced by photons reaching PMT.

The whole process can be summarized in the following algorithm:

1. Based on the path length of a particle inside the scintillator, the number of created photons can be obtained.
2. Then, a random direction (θ and φ) is assigned to each photon.
3. The photon path is followed until it hits the surface of the scintillator. If θ is greater than the critical angle, it will undergo total internal reflection, i.e., it will be mirrored inside the scintillator. Otherwise, it will get out of the scintillator. By using the geometry of the detector (pyramidal shape of the light enclosure) and equations of the detector surfaces, distance between start point and hit point of the photon with one of the light enclosure surfaces is calculated.
4. At this stage, four different cases can happen:
 - a. the photon is attenuated inside the scintillator,
 - b. the photon is absorbed in one of the surfaces,
 - c. the photon reaches PMT, or
 - d. the photon is still alive and should be followed up.

In the cases a and b the photon is not counted, and should be put away. If a photon reaches the PMT, the flight time will be saved. Otherwise, in case d, the photon is not absorbed in the surfaces and it should be reflected in a new random direction, so we go back to step 2. For photons reaching PMT, the emission time also should be added to the time of flight. If for any reason the photon does not reach the PMT after 200 ns, the program does not follow this photon, and goes to the next photon.

To consider the absorption of photons in the walls and the bottom surface of the light enclosure, a generated uniform random number $R \in [0, 1]$ is compared with the absorption coefficients of the walls (0.2) and the surface (0.1). If R is less than the absorption coefficient, this photon is considered as absorbed. Similarly, for the attenuation of the photons in the scintillator, another

Photon statistics	Number	%
Photons emitted in the Scintillator	41280	100
Photons reaching PMT	484	1
Photons attenuated inside the scintillator	15357	37
Photons absorbed on the bottom surface of the light enclosure	15349	37
Photons absorbed on the walls of the light enclosure	10090	25

Table 2: Total number of photons emitted from the scintillator, number of photons reaching PMT, attenuated inside the scintillator, absorbed on the bottom surface of the light enclosure and absorbed on the walls of the 20 cm light enclosure.

uniform random number should be compared with the attenuation probability distribution, which is given by $P_{\text{att.}}$:

$$P_{\text{att.}} = 1 - e^{-l/\lambda}; \quad (4)$$

where l is the distance traveled by the photon inside the scintillator, and $\lambda = 250$ cm is the attenuation length of photons in the NE102A [14].

3.2. Results and discussion

When a charged particle passes through the detector, on average, 41280 photons will be emitted from the scintillator. A small fraction of them reach the PMT, and most of them will be either absorbed on the light enclosure surface or attenuated inside the scintillator. Table 2 gives the results of our extended-code simulation about the fate of the photons emitted from the scintillator in the light enclosure with a height of 20 cm. The given values in table 2 are the mean number of photons of all the cells on the scintillator surface with repeating the simulation 200 times for each cell. According to the number of photons reaching PMT (485 photons), the photon collection efficiency is $\sim 1\%$. This is consistent with scintillators with WLS fiber readouts, since a large fraction of the emitted photons will be lost in the process of photon absorption and re-emission in WLS fibers. For example, the photon collection efficiency of the scintillation detectors of GRAPES-3 with WLS fibers obtained by G3Sim code is $\sim 0.4\%$ [20].

It is informative to consider number of collisions of counted photons (i.e., the photons reaching PMT) with the walls of the light enclosure. Among photons reaching PMT, some of them do not collide with the walls of the light enclosure, and the rest collide once, twice or more with the walls. Table 3 presents number of photons reaching PMT for different numbers of collisions with the walls.

More than half of the counted photons collide the walls less than 4 times, and for more than 15 collisions, the number of counted photons is less than 0.1% (third column of Table 3). On average 75 photons reach PMT without any collision with the walls or the bottom surface of the light enclosure. This number of photons is enough to produce a signal in PMT. For a typical PMT with quantum efficiency of $\sim 28\%$, an output signal could be produced by ~ 21 photoelectrons.

No. of collisions	No. of photons	%
0	75	15.5
1	74	15.3
2	61	12.6
3	51	10.5
4	42	8.7
5	35	7.2
6	28	5.8
7	22	4.6
8	18	3.7
9	15	3.1
10	12	2.5
11	8	1.7
12	6	1.2
13	5	1.0
14	4	0.1
15	4	0.1

Table 3: Counted photons with different numbers of collisions with the walls, averaged over 200 runs, for the cell 3 of the 20 cm light enclosure.

The time spectrum of photons, i.e., the number of photons reaching PMT in 0.5 ns time intervals, gives a very valuable information about the performance of the detector. The total number of photons reaching PMT (the area under the spectrum curve), the rise time, the FWHM, the fall time, and the shape of the spectrum provide suitable tools to compare the detectors with different light enclosure heights. Time spectra of 3 light enclosure heights corresponding to the third cell (Fig. 1(c)) are shown in Fig. 5. Increasing height of the light enclosure has multiple effects on the spectrum: it shifts the whole spectrum and its maximum toward the later times; it decreases the height of the spectrum; and it increases the rise time and FWHM.

The mean rise time of the spectra of 200 runs for each cell of the detector is plotted as a function of distance from the PMT in Fig. 6. The rise time at the center of the detector is minimum and increases by going toward the corner. The smallest value for the rise times belong to the 10 cm light enclosure in all cells, and the corresponding values increase by increasing the light enclosure height. On the other hand, the slopes of the fitted lines, in Fig. 6, show that the rise time of the 10 cm light enclosure is more non-uniform.

Dispersion of the rise times around the average value gives time resolution of the detector. These values are 0.11 ns, 0.10 ns, and 0.13 ns for 10 cm, 20 cm, and 30 cm light enclosures, respectively. On the other hand, the time resolution of the 20 cm light enclosure is obtained by experiment. Error of the time measurement can be represented by $\sigma_{\text{total}} = (\sigma_{\text{elec.}}^2 + \sigma_{\text{d}}^2)^{0.5}$, where $\sigma_{\text{elec.}}$ and σ_{d} are, respectively, the errors in time due to the electronic circuit and the detector (including the light enclosure and the scintillator). Since σ_{total} and σ_{d}

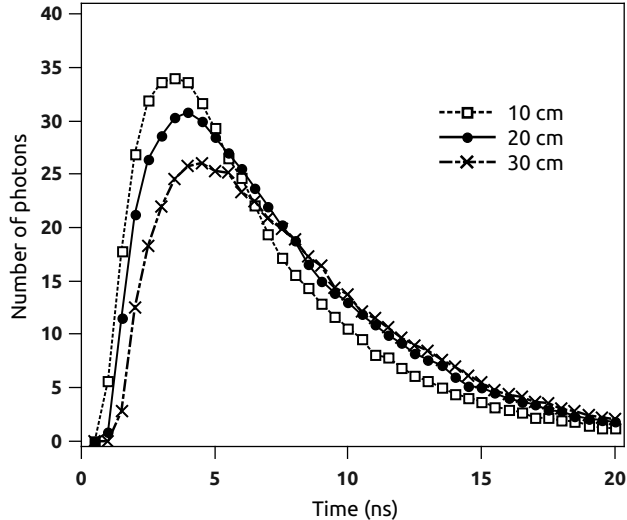


Figure 5: Time spectrum of photons reaching PMT corresponding to cell 3 for 3 light enclosures.

are 1.85 ns and 0.10 ns, respectively, we obtain $\sigma_{elec.} = 1.847$ ns. The latter error is due to 2 PMTs, 2 discriminators, one TAC and one ADC in the circuit. The timing errors (by catalogues) of the PMT, the discriminator, the TAC, and ADC are 1.27 ns, 0.1 ns, 0.1 ns, and 0.2 ns, respectively. On the basis of these errors, the total electronic error is

$$\sigma_{elec.} = (2\sigma_{PMT}^2 + 2\sigma_{Disc}^2 + \sigma_{TAC}^2 + \sigma_{ADC}^2)^{0.5} = 1.82 \text{ ns}; \quad (5)$$

Therefore, the time resolution of the detector is $\sigma_d = (\sigma_{total}^2 - \sigma_{elec.}^2)^{0.5} = 0.31$ ns, which is comparable with 0.10 ns of simulation.

Regardless of these considerations, there is a general conclusion which is consistent with the experimental results: increasing the height of the light enclosure improves the uniformity of the rise time while decreasing the height diminishes the rise time values.

Fig. 7 gives total number of photons reaching PMT, averaged over 200 runs, as a function of distance between corresponding cell and PMT. When the number of photons reaching PMT exceeds a certain value, the efficiency will be 100%. Below this value, a little change in the number of photons reaching PMT may affect the efficiency. For the 10 cm light enclosure, when an ionizing particle passes through the center of the detector (cell 1 of Fig. 1(c)), more than 1300 photons are counted in PMT. This is much more than the values related to other cells and other light enclosure heights. This means that it is reasonable to estimate the efficiencies of the detectors in terms of the efficiency of the cell 1 in the 10 cm light enclosure height as given in Table 1.

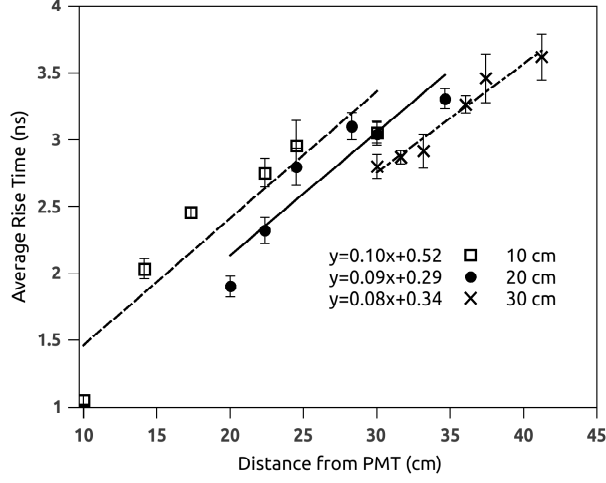


Figure 6: Rise time of 6 cells as a function of distance between corresponding cell and PMT for 3 light enclosures. The values are averaged over 200 runs of the program. Fitted lines and their slopes are given in the graph for 10 cm , 20 cm, and 30 cm light enclosures. Deviation of rise time points from the fitted lines could be result of light enclosures geometric asymmetry.

We can estimate the response of each detector in terms of photons reaching PMT. If the threshold height of the signal in the discriminator is V_0 , for recording an event, the generated signal in PMT should have a pulse height more than V_0 . The output of PMT is a current, I_p , while the external signal is a voltage. For converting the current output of a PMT into a voltage output, a load resistance R_L is used. This current for voltage V_0 is given by $I_{0p} = V_0/R_L$. On the other hand, the current is

$$I_p = \frac{dQ}{dt} = G e \frac{dN_{p.e.}}{dt} = G e \eta \frac{N_{ph}}{\tau}; \quad (6)$$

where G is the gain of PMT ($\sim 10^8$), e is the electron charge, η is the quantum efficiency of the photocathode ($\sim 28\%$), $\frac{dN_{p.e.}}{dt}$ is the rate of photoelectrons produced in the photocathode, N_{ph} is the number of photons reaching PMT, and τ is the decay time constant of the scintillator (~ 2.5 ns).

We can obtain N_{ph} from the current ($I_p = V/R_L$) and the other parameters. We denote the number of photons reaching PMT, corresponding to I_{0p} , by N_{0ph} . Now, if $N_{ph} > N_{0ph}$, the signal is recorded, otherwise it is not recorded. Thus, the response of the detector is estimated.

3.3. Geant4 cross check

To cross check our extended-code simulation, an another simulation was performed using the Geant4 toolkit [17], only for the 20 cm light enclosure. To converge the results, we had to modify our extended-code simulation. As it was

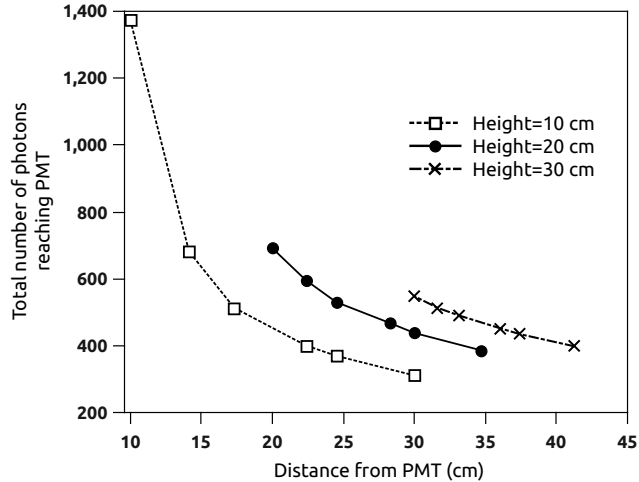


Figure 7: Total number of photons reaching PMT as a function of distance between corresponding cell and PMT for 3 light enclosures. The numbers are averaged over 200 runs of the program. Since the error bars are smaller than the data points, they are omitted.

mentioned in §3.1, in our extended-code simulation, for dE/dx and dN/dl we used the values 2 MeV/cm and $20,000\text{ photons/cm}$, respectively. These values are reasonable for MIP in a low- Z material, but are not reasonable for NE102A. In the Geant4 simulation, for the scintillator NE102A, the H/C ratio (number of the hydrogen atoms to carbon atoms) is considered to be 1.105 [19]. This means that the total number of photons emitted from each 1 cm of the scintillator, in extended code, is set to have the same value as that of a 1 GeV electron obtained by Geant4. To converge the results of the two simulations, we have to normalize the number of emitted photons.

Fig. 8 shows the photon spectrum of the Geant4 and Extended-code simulations for the cell 3 of a 20 cm light enclosure. The spectrum of Geant4 is the result of 200 times running of the code and of extended-code 300 times. There is a good agreement between the results of the two simulations.

4. Conclusion

The experiment in cosmic ray laboratory at Sharif University of Technology shows that the 20 cm height is almost an optimum height for the light enclosures of the Alborz-I scintillators. This conclusion is confirmed by the extended-code and the Geant4 simulations. The simulations show that for the detectors of Alborz-I, only 1% of emitted photons from the scintillator can reach the PMT. Since the detectors of Alborz-I will be used for timing measurement and not for energy deposition of particles, shape and material of the light enclosure do not play an important role for these detectors. In order to use the detectors for

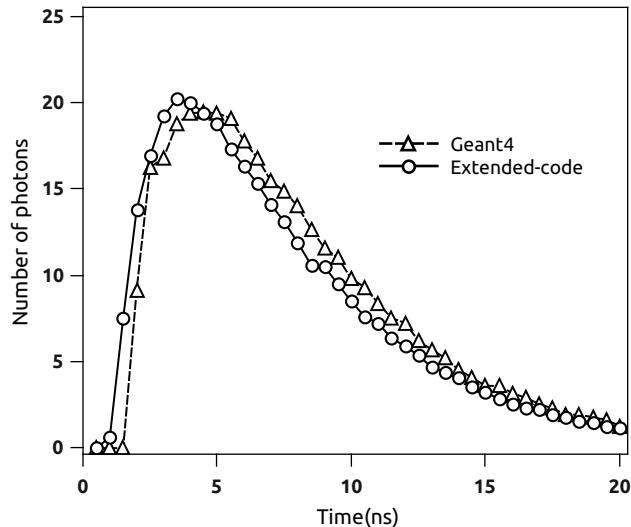


Figure 8: Time spectrum of photons: number of photons reaching PMT in 0.5 ns time intervals, obtained by Extended-code (300 times running) and Geant4 (200 times running) simulations corresponding to cell 3 of a 20 cm light enclosure.

measurement of energy deposition, the uniformity plays an important role and using the WLS fiber readouts is a better choice. This is the case for the current experiments — such as new generation detectors of GRAPES3 [18], shielded plastic scintillators of KASCADE experiment for detection of muons [3], and electromagnetic detectors of LHAASO-KM2A [21] — which use scintillators for detection. Total time resolution of the Alborz-I detectors, including the scintillator, the light enclosure, and the PMT, is found to be 1.31 ns. This time resolution fully satisfies our needs for studying the extensive air showers by the timing methods.

5. Acknowledgements

The authors wish to express their gratitude to all members of Samimi Cosmic Ray Laboratory (SCRL), specially Saba Mortazavi Moghaddam for her help in doing experiments, Hadi Hedayati for his help in the first version of extended-code simulation, Soheila Abdollahi and Mr. Orami for their help and support. Mohsen Akbari, Ahmad Shariati, Amir Aghamohammadi and Encieh Erfani are thanked for numerous constructive comments. The authors are very grateful for the invaluable and constructive comments of the anonymous referees.

References

- [1] E. S. Seo, Direct measurements of cosmic rays using balloon borne experiments, *Astroparticle Physics* 39–40 (2012) 76–87.
- [2] M. Wurm, et al., The next-generation liquid-scintillator neutrino observatory lona, *Astroparticle Physics* 35 (2011) 685–732.
- [3] T. Antoni, et al., The cosmic-ray experiment kascade, *Nuclear Instruments and Methods in Physics Research A* 513 (2003) 490–510.
- [4] T. Abu-Zayyad, et al., *Nuclear Instruments and Methods in Physics Research A* 689 (2012) 87–97.
- [5] W. D. Apel, et al., The kascade-grande experiment, *Nuclear Instruments and Methods in Physics Research A* 620 (2010) 202–216.
- [6] Shuwang Cui, Ye Liu, Yujuan Liu, Xinhua Ma, Simulation on gamma ray astronomy research with LHAASO-KM2A, *Astroparticle Physics* 45 (2014) 86–92.
- [7] M. Amenomori, et al., Cosmic-ray energy spectrum with the tibet air-shower experiment, *Astrophysics Space Science Transactions* 7 (2011) 15–20.
- [8] S. K. Gupta, et al., Grapes-3 a high-density air shower array for studies on the structure in the cosmic-ray energy spectrum near the knee, *Nuclear Instruments and Methods in Physics Research A* 540 (2005) 311–323.
- [9] S. Mortazavi, et al., *Astroparticle Physics* 94 (2012) 22.
- [10] M. Bahmanabadi, et al., A study of the effect of geomagnetic field on extensive air showers with small arrays, *Experimental Astronomy* 13(1) (2002) 39–57.
- [11] M. Bahmanabadi, et al., An investigation on anisotropy of cosmic rays with a small air shower array, *Experimental Astronomy* 15 (2003) 13–27.
- [12] M. Khakian Ghomi, M. Bahmanabadi and J. Samimi, Observation of EGRET Gamma-Ray Sources by an Extensive Air Shower Experiment, *Astronomy and Astrophysics* 434 (2002) 459-467.
- [13] M. Bahmanabadi, et al., comparison of the performance of various light enclosures for extensive air shower experiments, *Experimental Astronomy* 8 (1998) 211–229.
- [14] G. F. Knoll, *Radiation Detection and Measurement*, 3rd Edition, John Wiley and Sons, Inc., 2000.
- [15] C. Grupen, B. Shwartz, *Particle Detectors*, 2nd Edition, Cambridge University Press, 2008.

- [16] W. R. Leo, *Techniques of Nuclear and Particle Physics Experiments*, Springer-Verlag, 1987.
- [17] J. Allison, et al., Geant4 developments and applications, *IEEE Transactions on Nuclear Science* 53 (2006) 270–278, DOI: 10.1109/TNS.2006.869826.
- [18] P. K. Mohanty, et al., Measurement of some eas properties using new scintillator detectors developed for the grapes-3 experiment, *Astroparticle Physics* 31 (2009) 24–36.
- [19] C. Leroy and P. G. Rancoita, *Principles of Radiation Interaction in Matter and Detection*, World Scientific, 2004.
- [20] P. K. Mohanty, S. R. Dugad and S. K. Gupta, Monte Carlo code G3sim for simulation of plastic scintillator detectors with wavelength shifter fiber readout, *Review of Scientific Instruments* 83 (2012) 043301
- [21] J. Zhao, et al., Design and performances of electromagnetic particle detector for LHAASO-KM2A, *Chinese Physics C* 38, (2014) 036002